



# NIH Public Access

## Author Manuscript

*Biomacromolecules*. Author manuscript; available in PMC 2012 December 12.

Published in final edited form as:

*Biomacromolecules*. 2011 December 12; 12(12): 4373–4385. doi:10.1021/bm201360v.

## Poly(2-aminoethyl methacrylate) with well-defined chain-length for DNA vaccine delivery to dendritic cells

Weihang Ji<sup>1,#</sup>, David Panus<sup>1,#</sup>, R. Noelle Palumbo<sup>1</sup>, Rupei Tang<sup>2</sup>, and Chun Wang<sup>1,\*</sup>

<sup>1</sup>Department of Biomedical Engineering, University of Minnesota, 7-105 Hasselmo Hall, 312 Church Street S. E., Minneapolis, MN 55455, USA

<sup>2</sup>School of Medicine and Pharmaceutics, Jiangnan University, 1800 Lihu Road, Wuxi 214122, P. R. China

### Abstract

Poly(2-aminoethyl methacrylate) (PAEM) homopolymers with defined chain-length and narrow molecular weight distribution were synthesized using atom transfer radical polymerization (ATRP), and a comprehensive study was conducted to evaluate the colloidal properties of PAEM/plasmid DNA polyplexes, the uptake and subcellular trafficking of polyplexes in antigen-presenting dendritic cells (DCs), and the biological performance of PAEM as a potential DNA vaccine carrier. PAEM of different chain-length (45, 75 and 150 repeating units) showed varying strength in condensing plasmid DNA into narrowly dispersed nanoparticles with very low cytotoxicity. Longer polymer chain-length resulted in higher levels of overall cellular uptake and nuclear uptake of plasmid DNA, but shorter polymer chains favored intracellular and intra-nuclear release of free plasmid from the polyplexes. Despite its simple chemical structure, PAEM transfected DCs very efficiently in vitro in media with or without serum and led to phenotypic maturation of DCs. When a model antigen-encoding ovalbumin plasmid was used, transfected DCs stimulated the activation of naïve CD8<sup>+</sup> T cells to produce high levels of interferon- $\gamma$ . The efficiency of transfection, DC maturation, and CD8<sup>+</sup> T cell activation showed varying degrees of polymer chain-length dependence. These structurally defined cationic polymers may have much potential as efficient DNA vaccine carriers and immunostimulatory adjuvants. They may also serve as a model material system for elucidating structural and intracellular mechanisms of polymer-mediated DNA vaccine delivery.

### INTRODUCTION

In recent years DNA vaccines have shown considerable promise for numerous medical interventions – from prophylactic vaccine strategies that target viral, bacterial or parasitic infections to potential therapeutics for treating infectious diseases, cancer, and autoimmune disorders<sup>1</sup>. DNA vaccination has advantages over conventional vaccines because of its simplicity, flexibility and safety. A plasmid DNA that encodes for a protein antigen of interest is the basic component of a DNA vaccine formulation. Ideally, antigen-presenting cells (APCs) transfected with the DNA vaccine should express the encoded antigen endogenously, process and present the antigenic peptide fragments through the Major Histocompatibility Complex (MHC) molecules, resulting in the generation of antigen-specific immune responses. The most important APCs, the dendritic cells (DCs)<sup>2</sup>, are widely

\*Corresponding author. Telephone: 612-626-3990; Fax: 612-626-6583; wangx504@umn.edu.

#W. Ji and D. Panus contributed equally to this work

Supporting Information Available: Results of CoV calculation, zeta-potential measurements, luciferase control for GFP transfection, FRET data, time course of gene transfection. This material is available free of charge via the Internet at <http://pub.acs.org>.

considered the ideal target cells of DNA vaccines. Sustained antigen presentation from DCs combined with DC maturation is expected to generate robust adaptive cellular immunity, which is particularly necessary for combating cancer and viral infection<sup>3</sup>.

A large number of cationic polymers with diverse structures and properties have been developed for gene delivery<sup>4–6</sup>, some of which have been evaluated for DNA vaccine delivery<sup>7</sup>. Despite much effort in the past, designing polymers as DNA vaccine carriers has been complicated due to vast possible combinations of physico-chemical variables and by the complex biological/immunological environment in which the carriers are used. For many years the molecular weight, or chain-length, of polymers has been shown to have significant impact on DNA delivery. The relationship between polymer molecular weight and transfection efficiency has been studied in many polymers such as branched polyethylenimine (PEI)<sup>8</sup>, poly(2-dimethylaminoethyl methacrylate) (PDMAEMA)<sup>9</sup>, trehalose oligoethylenamine click polymers<sup>10</sup>, and polyphosphoramidate (PPA)<sup>11</sup>, to name a few. In general, increasing molecular weight will increase gene expression. However, some discrepancies exist<sup>8, 12, 13</sup> and fundamental understanding of the influence of linear polycation chain-length on the gene transfer process, especially in the context of DNA vaccine delivery to immune cells, remains elusive.

Controlled polymerization techniques such as atom transfer radical polymerization (ATRP)<sup>14, 15</sup> make it possible to prepare cationic polymers with defined chain-length in a facile way. Recently we have synthesized polyethylene glycol-*block*-poly(2-aminoethyl methacrylate) (PEG-*b*-PAEM) diblock copolymers with narrow molecular weight distribution by ATRP and have shown that the length of the cationic block exerted significant influence on how the polymer carrier interacted with plasmid DNA and how the polyplexes interacted with DCs<sup>16</sup>. Although the PEG-*b*-PAEM diblock copolymers are useful model systems, they had low transgene expression efficiency in DCs, a significant drawback that limits their practical usage in DNA vaccination.

In this study we focused on poly(2-aminoethyl methacrylate) (PAEM) homopolymers with defined chain-length and narrow molecular weight distribution. We investigated comprehensively the colloidal properties of the PAEM/plasmid polyplexes (including stability, particles size and charge), uptake and subcellular trafficking in DCs, and biological/immunological properties in vitro (including cytotoxicity, transfection efficiency, DC maturation, and activation of naive CD8<sup>+</sup> T cells to produce interferon- $\gamma$ ), aiming to further elucidate the impact of polymer chain-length on DNA delivery to DCs and to evaluate the practical value of PAEM as DNA vaccine carrier and immunostimulatory adjuvant.

## EXPERIMENTAL SECTION

### Materials

Toluene (Sigma-Aldrich, St. Louis, MO) was dried by refluxing over sodium and distilled. *N*-(*tert*-butoxycarbonyl)aminoethyl methacrylate (*t*BAM) was synthesized as described<sup>17</sup>. Ethyl  $\alpha$ -bromoisobutyrate, copper (I) chloride (CuCl) and 2,2'-dipyridyl (bPy) were purchased from Sigma-Aldrich. 3-[4,5-Dimethylthiazol-2-yl]-2,5-diphenyltetrazolium bromide (MTT), Dulbecco's phosphate buffered saline (DPBS), Dulbecco's Modified Eagle's Medium (DMEM), fetal bovine serum (FBS), and trypsin were purchased from Invitrogen (Carlsbad, CA). Murine DC 2.4 cells (ATCC, Manassas, VA) were incubated in DMEM containing 10% FBS, 10 mM HEPES, 100 U/mL penicillin/streptomycin at 37°C and a humidified atmosphere containing 5% CO<sub>2</sub>. Three different DNA plasmids were used in various experiments: (1) a green fluorescent protein plasmid (pEGFP-N1), used for evaluating polyplex properties and gene transfection; (2) a firefly luciferase plasmid

(pCMV-Luc), used in cellular uptake and subcellular trafficking studies and as a negative control in transfection experiments; (3) a chicken ovalbumin plasmid (pCMV-OVA), used in DC maturation and CD8<sup>+</sup> T cell activation experiments. All three plasmids contained a CMV promoter. Other chemicals and solvents were purchased from Sigma-Aldrich and used without further purification.

### Synthesis of poly(2-aminoethyl methacrylate) (PAEM)

The ATRP of *t*BAM followed a procedure modified from Tang *et al*<sup>16</sup>. A glass two-neck flask was charged with *t*BAM, CuCl, bPy, and the system was degassed three times. Dried degassed toluene and ethyl α-bromoisobutyrate as initiator were added, and the mixture was heated at 80°C for 8 h. The reaction was terminated by exposing the system to air. The reaction solution was then diluted by dichloromethane and passed through a basic aluminum oxide column to remove the copper complex. The product was precipitated in hexane twice and dried in vacuum at room temperature for 2 days. Three different monomer-to-initiator feed ratios (50:1, 100:1, 200:1) were used to obtain PtBAM homopolymers with varying chain-length. To remove the Boc groups, 0.8 g of PtBAM was dissolved in 5 mL of trifluoroacetic acid (TFA) and stirred for 2 h at room temperature. TFA was then removed by evaporation, and the oil residue was rinsed three times with diethyl ether. The resultant precipitate was collected by filtration, washed twice by diethyl ether, and dried overnight in vacuum. The polymers were then washed with NaOH water solution at pH 9.0, and dialyzed (MWCO 3,500) against distilled deionized water for 3 days. The final PAEM polymers were obtained by lyophilization.

### Characterization of polymers

The <sup>1</sup>H and <sup>13</sup>C NMR spectra of the polymers were acquired on a Varian Unity spectrometer (300 MHz) using CDCl<sub>3</sub> (for PtBAM) and D<sub>2</sub>O (for PAEM) as solvents. Chemical shifts were recorded in ppm and referenced against tetramethylsilane (TMS) and D<sub>2</sub>O, respectively. Gel Permeation Chromatography (GPC) experiments to analyze PtBAM were performed at 35°C in CHCl<sub>3</sub> with a flow rate of 1 mL/min using a Hewlett-Packard 1100 series liquid chromatography equipped with three PL gel 5-μm mixed columns (Jordi Gel columns of 500, 103, and 104 Å pore sizes) and a Hewlett-Packard 1047A refractive index detector. The GPC instrument was calibrated with polystyrene standards (Polymer Laboratories, Amherst, MA). All sample solutions were filtered through a 0.22-μm filter before analysis.

### Gel retardation assay

Polyplexes of N:P ratios ranging from 1/8 to 16 were prepared by adding 25 μL of polymer solution in 20 mM HEPES (pH 7.4) to 25 μL of DNA plasmid solution (0.2 μg/μL in 20 mM HEPES, pH 7.4) vortexed for 10 s, incubated for 30 min at room temperature, and analyzed by electrophoresis on a 1.0% agarose gel containing 0.5 μg/mL ethidium bromide.

### Heparin competition assay

To determine the strength of DNA binding by polymers with varying chain-length, polyplexes at N:P ratio of 8 were incubated with increasing concentrations of heparin (0.1 to 0.9 IU per μg of DNA) for 20 min at room temperature and analyzed by agarose gel electrophoresis.

### Ethidium bromide (EB) exclusion

Polymer solutions were added to pre-mixed EB and plasmid solution with varying N:P ratios from 1/8 to 32 and incubated for 30 min. The intensity of EB fluorescence was recorded by

a Bio-Tek Synergy HT plate reader with excitation wavelength of 530/25 nm and emission wavelength of 590/35 nm. DNA/EB solution without any polymer was used as a control.

### Dynamic light scattering (DLS) and zeta potential measurement

The average hydrodynamic diameter and polydispersity index of polyplexes in HEPES buffer (20 mM) at 25°C were determined using a ZetaPlus Particle Analyzer (Brookhaven Instruments Corporation, Holtsville, NY; 27 mW laser; 658 nm incident beam, 90° scattering angle). Polyplexes with N:P ratios ranging from 1/4 to 32 were prepared as described above and diluted 20 times to a final volume of 2 mL in HEPES buffer before measurement. Simultaneously the zeta-potential of the polyplexes was determined using the ZetaPal module of the Particle Analyzer.

### Transmission electron microscopy (TEM)

The morphology and size of polyplexes at N:P ratio of 8 were observed using a JEOL 1200 EXII transmission electron microscope. Samples for TEM were prepared by placing a drop of the polyplex solution onto carbon-coated EM grids followed by negative staining using phosphotungstic acid (1.0%, pH 4~5).

### Cytotoxicity assay

The cytotoxicity of free polymers was evaluated by a MTT (3-(4,5-dimethyl-thiazol-2-yl)-2,5-diphenyl tetrazolium bromide) assay<sup>18</sup>. DC 2.4 cells were seeded into 96-well plates at 6000 cells/well and cultured with polymers of various concentrations for 24 h in DC 2.4 media (DMEM low glucose, 10% FBS, 10 mM HEPES, 100 U/mL penicillin/streptomycin) at 5% CO<sub>2</sub> and 37°C. MTT in PBS (5 mg/mL, 20 µL) was added to each well reaching a final concentration of 0.5 mg/mL. After 4 h, unreacted MTT was removed by aspiration. The formazan crystals were dissolved in 150 µL of DMSO and the absorbance was measured at 570 nm using a Bio-Tek Synergy HT plate reader. Cell viability was calculated by [Absorbance of cells exposed to polymers]/[Absorbance of cells cultured without polymers] in percentage.

### Fluorescence labeling of polymer and plasmid

For subcellular trafficking studies, both the PAEM polymers and DNA plasmid were covalently labeled with fluorophores. PAEM was labeled with Oregon Green 488 carboxylic acid succinimidyl ester (Invitrogen) using a method previously described<sup>19</sup> followed by purification by dialysis (MWCO 3,500). The DNA plasmid was labeled with a Cy5 fluorophore using a MIRUS LabelIT Kit (Mirus, Madison, WI) according to manufacturer's protocol. After the labeling reaction, the DNA plasmid was purified from excess dye by means of ethanol precipitation according to the manufacturer's protocol. Both purified labeled PAEM polymer and DNA plasmid were stored at -20°C until use.

### Cellular uptake and subcellular trafficking

DC 2.4 cells were seeded in 4-well LabTek II glass chamber slides (Fisher Scientific, Pittsburgh, PA) at a density of 100,000 cells per well in 1 mL of media. To visualize cellular uptake and polyplex intracellular dissociation, polyplexes were formed using fluorescently labeled PAEM and luciferase plasmid. Prior to transfection, the DC 2.4 media was removed and the cells washed once with warm PBS and replaced with serum-free DC 2.4 cell media. Cells were incubated with polyplexes for 1, 4, or 24 h at 37°C, 99% humidity, and 5% CO<sub>2</sub>. For the 24-h samples, the serum-free media was removed after 4 h and the cells were washed twice with warm PBS and replaced with complete DC 2.4 media containing 10% serum and incubated for an additional 20 h. Prior to confocal microscopy imaging, Hoechst 33342 (Invitrogen) was added to each chamber at a final concentration of 30 µM to stain the

cell nuclei, and the samples were washed and fixed using BD cytofix fixation buffer (BD Bioscience, San Jose, CA) according to the manufacturer's protocol. The cells were then mounted with SlowFade Gold<sup>®</sup> anti-fade reagent (Invitrogen), covered with a coverslip, and sealed with clear nail polish. Cell images were captured with an Olympus FV-1000 confocal microscope equipped with an Olympus 60x/1.42 NA oil-immersion lens (Center Valley, PA). The fluorescence intensity of each fluorophore was adjusted using individual single-fluorophore positive and cell-only negative controls. The Cy5 label was excited at 643 nm and detection of emission was set at 670 nm. Hoechst 33342 was excited at 405 nm and emission detected at 451 nm. Imaging limits (z-slices) were set to collect the top and bottom boarders of the cells at a step size of 0.4  $\mu$ m and 800 pixel resolution. Images of at least three fields of view were collected for every sample.

Förster Resonance Energy Transfer (FRET) sensitized emission was used to verify the results of polyplex dissociation at 24 h obtained using 3-D fluorescence colocalization method. Prior to imaging, the PAEM polymers were labeled with Oregon Green-488 as described above, while the luciferase plasmid was labeled with Cy3 using a MIRUS LabelIT kit according to the manufacturer's protocol. Transfection of DC 2.4 cells were carried out according to the same procedures described above. DC 2.4 cells were also transfected with FRET controls consisting of non-labeled PAEM complexed with Cy3-plasmid and Oregon Green-488 labeled PAEM complexed with non-labeled plasmid in separate individual wells. After 24 h, cells were washed with PBS, fixed with BD-Cytofix according to the manufacturer's protocol, mounted using SlowFade Gold anti-fade media, and fluorescence images were acquired. Three different fields of view were imaged for each of the FRET control and FRET polyplex samples according to the Olympus sensitized emission FRET protocol.

To determine endolysosomal colocalization, DC 2.4 cells were transfected with polyplexes formed with non-labeled PAEM and Cy5-labeled luciferase plasmid. Thirty minutes prior to imaging, cells were stained with Hoechst 33342 for 20 min followed by Lysotracker Green DND-26 (Invitrogen) at a final concentration of 100 nM according to manufacturer's protocol. The cells were then washed with PBS and mounted with ascorbic acid at a final concentration of 5  $\mu$ M to minimize photo-bleaching. The Lysotracker Green fluorochrome was excited at 488 nm and emission detected at 520 nm. All samples were kept on ice until imaged.

### Image analysis and quantification

The confocal fluorescence microscopy images of cellular uptake and subcellular trafficking were analyzed using ImageJ software and image quantification was carried out using a method developed by Akita *et al*<sup>20</sup>. Imported confocal images were opened in individual color components and converted to 8-bit images. Individual cells used for the analysis were then randomly isolated from each image. Cellular uptake of Cy5-labeled plasmid was measured by individually thresholding the z-slices of each cell and calculating the total pixel area within a region of interest (ROI) drawn around the cell membrane. Polyplex intracellular dissociation was quantified by measuring the degree of colocalization between Oregon Green 488 labeled PAEM and Cy5 labeled plasmid. Each complex component was thresholded individually for each z-slice. The total pixel area of the Cy5-plasmid signal was calculated. Colocalization of the two fluorophores was measured as the spatial overlap between the two individual thresholded images in the unit of total pixel area, using the ImageJ colocalization plug-in. The percentage of polyplex dissociation was determined as one subtracting the ratio between the Oregon Green/Cy5 colocalized total pixel area and the total Cy5 pixel area. The same 3-D fluorescence colocalization method was applied to determining the percentage of endolysosomal colocalization. All FRET images were analyzed and quantified using the FV-ASW 1.5 software and precision FRET (pFRET)

sensitized emission function. The software analyzed the median z-slice of the cells and reported images of the Oregon Green-488 PAEM sample emission, Cy3 plasmid sample emission, and the polyplex pFRET. Nuclear localization of plasmid was quantified by calculating the total pixel area of Cy5 plasmid within a ROI of the nuclear membrane. The geometry of nuclei was determined by stacking the z-slices into 3-D images and orthogonal views to verify that the Cy5-plasmid signal was indeed within the boundary of the nucleus. A total of 30 cells were analyzed for each experimental group based on the coefficient of variance<sup>20</sup> (Supporting information, Figure S1). Note that fluorescence intensity of all the images was not adjusted in ImageJ prior to quantification.

### Gene transfection in vitro

DC 2.4 cells were seeded into 12-well plates at 100,000 cells/well and cultured overnight. For transfection under serum-free condition, the cell media was removed and cells washed by PBS twice followed by adding DC 2.4 media without serum. Transfection with polyplexes of the GFP plasmid lasted for 4 h at 5% CO<sub>2</sub> and 37°C. The media was then discarded, cells washed by PBS twice, and cultured in serum-containing media for another 20 h before GFP level was recorded. For transfection in media containing 10% serum, DC 2.4 cells were incubated with polyplexes for 24 h at 5% CO<sub>2</sub> and 37°C. The cells were harvested by treating with trypsin-EDTA, dispersed in FACS buffer (PBS containing 1% bovine serum albumin), and analyzed using a BD LSR II flow cytometer. DC 2.4 cells were also transfected by polyplexes of the luciferase plasmid under the same conditions to exclude the autofluorescence of cells. Percentage of GFP<sup>+</sup> cells was determined using Flowjo. The GFP positive gate was drawn based on the luciferase control where false positive frequency was restricted to below 0.2%.

### DC maturation

DC 2.4 cells were transfected with polyplexes at N:P ratios of 8 and 16 as described above. Twenty-four hours later, the cells were stained with PE-labeled anti-mouse-CD40 antibody (Biolegend, San Diego, CA) and analyzed by flow cytometry. Untreated cells were of the immature phenotype (iDC, CD40<sup>low</sup>). Positive mature DCs were generated by stimulating with 2 µg/mL of lipopolysaccharide (LPS, from *E. coli* strain 026:B6, Sigma). All cell culture media, buffers, polymer stock solutions, and plasmid stock solution were tested free of endotoxin contamination using a LAL endotoxin detection kit following manufacturer's instruction.

### CD8<sup>+</sup> T cell activation

Naïve mouse CD8<sup>+</sup> T cells from the lymph nodes of OT-1/PL TCR transgenic mice were isolated as described previously<sup>21</sup>. To determine T cell activation, DC 2.4 cells were transfected using polyplexes containing an OVA plasmid with or without serum for 24 h as described above. Lymph node cells from OT-1/PL TCR transgenic mouse were added to the DCs so that approximately  $3 \times 10^5$  CD8<sup>+</sup> T cells were present in each well. After co-culturing for 3 days, the supernatant of the cell media was analyzed for IFN-γ by ELISA using a Ready-Set-Go IFN-γ "Femto-HS" kit (e-Bioscience, San Diego, CA) following manufacturer's procedure. As a positive control, iDCs without transfection were stimulated with SIINFEKL peptide (New England Peptide, LLC., Gardner, MA) at 1 µM for 1 h and with LPS at 2 µg/mL overnight before T cells were added.

### Statistical analysis

Statistical analysis was carried out using a two-sample Student's *t*-test with unequal variance. Values of *p*<0.05 were deemed to be different with statistical significance.

## RESULTS AND DISCUSSION

### Synthesis and characterization of PAEM homopolymers

We have chosen a simple cationic polymer, PAEM, as a model carrier for DNA vaccine delivery. The repeating unit of PAEM contains a primary amine in the side-chain (Figure 1A), which is capable of condensing efficiently any anionic cargos including plasmid DNA. PAEM has been used to prepare copolymers to study properties of polyion complex micelles with heparin<sup>22</sup> or oligodeoxynucleotide<sup>23</sup>, to deliver genes to COS cells in vitro<sup>24, 25</sup>, or to serve as antimicrobial agents<sup>17</sup>. Recently, we have reported on a series of well-defined diblock copolymers of PEG and PAEM that can condense and deliver plasmid DNA to DC 2.4 cells and have shown that the length of the PAEM block had much influence on the properties of the polyplexes, gene transfection efficiency, and DC maturation<sup>16</sup>. However, due to the presence of the PEG block, the diblock copolymers had rather low transfection efficiency, which poses a potential limitation to practical application of the polymers for DNA vaccination. To this end, here we have synthesized PAEM homopolymers with well-defined chain-length and conducted a comprehensive investigation on the physico-chemical properties of the polyplexes, polyplex/DC interaction including subcellular trafficking, efficiency of transfection, phenotypic maturation of DCs, and CD8<sup>+</sup> T cell stimulation in vitro.

PAEM was synthesized using ATRP modified slightly from a previously described process<sup>16</sup>. In the first step, the ATRP of Boc-protected aminoethyl methacrylate monomer (*t*BMA) was initiated by ethyl  $\alpha$ -bromoisobutyrate with Cu(I)-dipyridyl complex as catalyst. The molar ratio of the monomer and initiator in the feed was varied to achieve PtBAM with different chain-length. Three PtBMA polymers were synthesized with monomer conversion of over 99% (determined by proton NMR, data not shown) and yield of over 70%. GPC traces showed single peaks (Figure 1B) and the number average molecular weight ( $M_n$ ) of the three polymers was calculated to be 0.98, 1.66 and  $3.37 \times 10^4$  with the polydispersity index (PDI) of 1.19, 1.20, and 1.16, respectively. The narrow molecular weight distribution of the polymers indicated that the ATRP reaction was successful. Proton NMR analysis (not shown) confirms the chemical structure of all three PtBAM polymers. The average degree of polymerization (DP) of the PtBAM was calculated to be 45, 75, and 150 based on GPC analysis (Figure 1B), and the three polymers were thus named PtBAM<sub>45</sub>, PtBAM<sub>75</sub>, PtBAM<sub>150</sub>, respectively. In the second step, the Boc protecting group was removed by TFA treatment. Proton NMR analysis (not shown) confirmed complete disappearance of the methyl proton signal of the Boc group at 1.46 ppm, proving that all the Boc groups have been removed. The final product was obtained by removing the TFA salt in a mild basic solution to give PAEM with free amines. During the TFA removal the pH was strictly controlled to be below 9 so as to prevent aminolysis of the methacrylate ester group<sup>26</sup>. Overall, this two-step synthesis possesses excellent control over the polymerization comparable to the recently reported single-step synthesis of PAEM<sup>26</sup>.

### The capacity of DNA binding and condensation is dependent on polymer chain-length

The gel retardation assay qualitatively revealed the difference in DNA binding ability among the three PAEM polymers. PAEM<sub>75</sub> and PAEM<sub>150</sub> were able to completely prevent the migration of plasmid DNA at the N:P ratio of 1 and beyond. However, at this neutral charge ratio, PAEM<sub>45</sub> could only partially retard the DNA migration and reach a complete retardation at N:P ratio of 2 (Figure 2A). EB exclusion experiment gave a more quantitative assessment of DNA condensation capacity of PAEM. As the chain-length of the polymers increased from DP of 45 to 150, the ability to condense plasmid DNA increased accordingly, judged by the lowering N:P ratios at which half of the EB was displaced from intercalating with DNA, resulting in reduced fluorescence intensity (Figure 2B).

The stability of polyplexes at N:P ratio of 8 was studied in the presence of increasing amount of heparin, a polyanion that can compete with DNA for the binding to the polycation, followed by agarose gel electrophoresis. As shown in Figure 2C, the threshold concentration of heparin at which polyplex disruption occurred was 0.4, 0.5, and 0.7 IU/ $\mu$ g of DNA for polyplexes of PAEM<sub>45</sub>, PAEM<sub>75</sub> and PAEM<sub>150</sub>, respectively, suggesting that polyplexes formed with longer PAEM chains were more stable than the short ones. This conclusion generally agrees with findings of other polydisperse cationic polymer carriers, such as PDMAEM<sup>9</sup>. Moreover, we have previously observed a similar trend in the PEG-*b*-PAEM/DNA complexes<sup>16</sup>. Interestingly, polyplexes formed with PEG-*b*-PAEM were more resistant against heparin destabilization than polyplexes formed with the PAEM homopolymer of the same chain-length. For example, with a DP of 75 the threshold heparin concentration was 0.8 IU/ $\mu$ g of DNA for the diblock and 0.5 IU/ $\mu$ g of DNA for the homopolymer. This difference is likely due to the steric hindrance to heparin posed by the PEG chains.

### Average particle size of the polyplexes and cytotoxicity are independent of polymer chain-length

The size of nanoparticles is highly important for gene delivery in general and potentially for DC targeting and internalization<sup>27</sup>. DLS revealed that regardless of PAEM chain-length, the average particle size of the polyplexes in aqueous buffer spanned a range of 100 to 200 nm with much dependence on the N:P ratio (Figure 3A). The size distribution of each type of polyplex was also quite narrow with PDI ranging from 0.05 to 0.2. The particle size peaked at around 170 nm at the neutral charge ratio. Decreasing or increasing the N:P ratio, the particle size decreased gradually. There's no distinct difference in particle size among the three PAEM polymers with different chain-length. TEM images supported the results of the DLS, showing typical spherical nanoparticles in a representative image of PAEM<sub>75</sub> polyplex at N:P ratio of 8:1 (Figure 3B). At N:P ratio of 8:1, polyplexes of PAEM of different chain-length also shared similar zeta potential values at around 35 mV (Supporting information, Figure S2). That the hydrodynamic size of polyplexes was independent of the molecular weight of polymers has been observed in other cationic polymer systems, such as poly(2-methyl-acrylic acid 2-[(2-(dimethylamino)-ethyl)-methyl-amino]-ethyl ester) (pDAMA) at N:P ratio >5<sup>28</sup> and trehalose click polymers at low N:P ratios<sup>10</sup>. This phenomena was also consistent with our previous report on polyplexes formed by PEG-*b*-PAEM and plasmid DNA, except at N:P ratio of 1, at which particle size decreased with increasing length of the PAEM block<sup>16</sup>.

Cytotoxicity of the PAEM polymers was evaluated using a murine dendritic cell line, DC 2.4. All the PAEM polymers regardless of chain-length were not toxic to DC 2.4 cells at concentrations as high as 10  $\mu$ g/mL (Figure 3C). Cell viability, determined by the MTT assay, dropped to around 70% at polymer concentration of 20  $\mu$ g/mL and to around 40% at 40  $\mu$ g/mL, but was still significantly less toxic than branched PEI (25 kD) at these concentrations. Overall, the cytotoxicity of PAEM polymers in DCs was not sensitive to changes of polymer chain-length, similar to what was observed with the PDMAEMA system<sup>9</sup>. It is noted that the subsequent subcellular trafficking studies were all conducted using polymer concentrations that were not toxic to cells.

### Longer PAEM chains enhance cellular uptake of polyplexes

Cy5-labeled luciferase plasmid complexed with non-labeled PAEM of different chain-length at the N:P ratio of 8 was used to visualize cellular uptake in DC 2.4 cells after 1, 4, and 24 h by confocal fluorescence microscopy (Figure 4A). The level of Cy5-plasmid fluorescence inside cells was then quantified based on the confocal images using a method reported by Akita *et al*<sup>20</sup> (Figure 4B). The confocal images showed that cellular uptake of the plasmid

began within the first hour of transfection, with all three PAEM chain-lengths resulting in similar quantities of Cy5-plasmid inside the cells. By 4 h and 24 h the amount of plasmid taken up by the cells continued to rise and there was clearly a dependence on chain-length. The quantity of cellular uptake of plasmid complexed to PAEM<sub>150</sub> was significantly ( $p < 0.05$ ) higher than that of either PAEM<sub>75</sub> or PAEM<sub>45</sub> at 4 h. The uptake of plasmid complexed to PAEM<sub>75</sub> arrived at a level similar to that of PAEM<sub>150</sub> polyplexes by 24 h, yet both remained significantly higher than the shorter PAEM<sub>45</sub> polyplexes (Figure 4B). These results indicate that the uptake of polyplexes by dendritic cells was more efficient when relatively longer cationic polymers were used. It is possible that longer cationic PAEM chains may form more stable polyplexes (demonstrated by Figure 2C), which might interact with the cell membrane more strongly than polyplexes formed from shorter polymer chains, thus facilitating internalization into the cells<sup>29</sup>.

### Shorter PAEM chains facilitate intracellular dissociation of polyplexes

To achieve transgene expression, the DNA plasmid must dissociate from the polymer carrier at some point after being taken up by the cells. Here confocal fluorescence microscopy images were used to assess the effect of polymer chain-length on polyplex dissociation after internalization (Figure 5A), which was then quantified by measuring the spatial colocalization of fluorescence signals from the Cy5-labeled DNA plasmid and Oregon Green 488-labeled PAEM at various time points (Figure 5B). All three PAEM chain-lengths possessed similar levels of bound Cy5-plasmid (~75%) at 1 h. However, as time went by, the percentage of intact polyplexes decreased with the fastest rate of dissociation occurring with the shortest PAEM<sub>45</sub>. Four hours post-transfection the percentage of intact polyplexes of PAEM<sub>45</sub> dropped to below 70%. At 24 h a clear chain-length dependence of polyplex dissociation was established with the shortest PAEM<sub>45</sub> having the lowest fraction (53%) of intact polyplexes. Interestingly, the difference in dissociation between PAEM<sub>75</sub> and PAEM<sub>150</sub> polyplexes was not statistically significant, in spite of PAEM<sub>150</sub> being twice as long as PAEM<sub>75</sub> (Figure 5B). Overall, it appeared that within 24 h all three types of polyplexes experienced various degrees of dissociation inside cells. Shorter polymer chain-length favored polyplex dissociation more than longer chains due to weaker binding between short polymer chains and DNA, which was corroborated by the heparin competition experiment (Figure 2C). These results obtained by using a 3-D fluorescence colocalization method can be confirmed by FRET measurement (Supporting information, Figure S4), showing lower pFRET in polyplexes with shorter PAEM chains. These findings demonstrated the possibility of using polymers of defined chain-length to modulate the time course of polyplex dissociation, and in turn, to control transgene expression.

### Endolysosomal localization is not clearly dependent on polymer chain-length

The colocalization of Cy5-labeled plasmid DNA and endolysosome was observed by confocal fluorescence microscopy (Figure 6A) and quantified by calculating the amount of overlap between the fluorescent signals of Cy5 and LysoTracker Green, a marker for endolysosome (Figure 6B). Unlike cellular uptake and polyplex dissociation, there was no overall chain-length dependence for endolysosomal localization of the polyplexes. All three polymers showed similar level of endolysosomal entrapment at 1 h (around 25 to 35%, no statistical significant difference), which increased to approximately 55% by 24 h. Interestingly, with the exception of PAEM<sub>150</sub>, endolysosomal entrapment of PAEM<sub>45</sub> and PAEM<sub>75</sub> polyplexes increased from 1 to 24 h. It could be that the polyplexes escaped endosome as quickly as within the first hour of internalization, but they were recaptured by acidic subcellular vesicles (such as autophagosomes) at later times. Alternatively, rather than escaping from endosome, the majority of the polyplexes bypassed the endocytic pathway and were internalized via other (such as caveolae-mediated) pathways. The elucidation of the internalization mechanisms of the PAEM/DNA polyplexes will require further studies.

### Longer PAEM chains promote nuclear localization of polyplexes but do not favor the release of free plasmid

The efficiency of plasmid to be trafficked into the nucleus was observed by confocal fluorescence microscopy (Figure 7A) and quantified using the following three parameters: (1) the total fluorescence intensity of Cy5-plasmid (including the polyplexes and free plasmid) inside the nucleus; (2) the fluorescence intensity of free plasmid inside the nucleus; and (3) the number of cells with detectable fluorescence signal of the Cy5-plasmid (as polyplex or free) in the nucleus (Figure 7B). Care was taken to ensure that only Cy5-plasmid signals within the boundary of the nuclei was counted. One hour after transfection, there was a minute amount of Cy5-plasmid found in the nuclei of 1 or 2 cells out of a total of 30 individual cells examined. Four hours later, slightly more Cy5 signal was found in the nuclei of less than 10 cells. By 24 h, similar to what was seen with cellular uptake (Figure 4), the total amount of Cy5-plasmid localized within the nucleus exhibited a dependence on polymer chain-length, with PAEM<sub>75</sub> and PAEM<sub>150</sub> showing significantly higher ( $p < 0.05$ ) nuclear uptake than that of PAEM<sub>45</sub> (Figure 7B). More cells transfected using PAEM<sub>75</sub> and PAEM<sub>150</sub> were found with Cy5-plasmid in the nucleus (14 and 16 out of 30 cells, respectively) than PAEM<sub>45</sub> (10 out of 30 cells). More importantly, there was substantial amount of nuclear Cy5-plasmid that had apparently dissociated from the polymer carrier by 24 h (Figure 7B). Although the longest PAEM<sub>150</sub> delivered the highest amount of free Cy5-plasmid to the nucleus, the fraction of the free plasmid was below 0.5 – the smallest of the three polymers. Taken together, it appeared that longer PAEM chains promoted the overall cellular uptake and the subsequent nuclear uptake of plasmid, but if the polymer chain was too long, then the release of free plasmid from the polymer might be hindered. Because efficient transgene expression requires maximizing the amount of free plasmid in the nucleus, it may be more ideal to use a polymer with moderate chain-length (such as DP of 75) so as to facilitate both nuclear transport and dissociation of polyplexes inside the nucleus.

Shown are examples of cell nuclei containing free plasmid (“high”), polyplex-bound plasmid (“low”), or no plasmid (“none”). (B) A montage of z-slices of a cell nucleus. Arrows in frames 15~21 identify plasmid signal inside the nucleus. Arrows in frames 25~30 point to plasmid signal at the edge of nuclear membrane. (C) Quantification of amount of plasmid (free and polyplex-bound) localized in the cell nucleus. The top portion of the bars represents the amount of free plasmid. Mean  $\pm$  SE, 30 cells for each sample were counted, \* $p < 0.05$ . The numbers are the frequency of cells within a 30-cell population that contained positive signal of the plasmid inside their nuclei.

### Transfection of DCs in vitro with and without serum

PAEM-mediated transfection of DC 2.4 cells with a GFP plasmid was conducted in cell culture media in the absence or presence of 10% serum, and the expression level of GFP was determined by flow cytometry (Figure 8). To exclude any possible interference from cell autofluorescence, DCs transfected under identical conditions but using a luciferase plasmid served as negative controls to set the GFP<sup>+</sup> gate (Supporting information, Figure S3). Under serum-free conditions, transfection efficiency of DC 2.4 cells measured by the percentage of GFP<sup>+</sup> cells ranged from around 10% to 35% (Figure 8A) and was dependent on both polymer chain-length and N:P ratio (Figure 8B). Overall, longer polymer chain-length enabled higher transfection with the exception of the longest PAEM<sub>150</sub> at high N:P ratios (16 and 24). In particular, at N:P ratio of 8, the chain-length dependence of transfection appeared consistent with the amount of free (transcriptionally active) plasmid found in the cell nucleus (Figure 7B).

For transfection in serum-containing media, the overall transfection level was much lower than that in serum-free media at all N:P ratios tested, but longer chain-length at high N:P ratios (16 and 24) did achieve transfection as high as 10% (Figure 8A and C). Similar decrease in transfection efficiency due to the inference of serum has been reported for many cationic polymers with different molecular structures<sup>30–32</sup>, and the reason is often attributed to destabilization of polyplexes by serum proteins. We found that longest PAEM<sub>150</sub> was able to form the most stable polyplexes among the three polymers tested and that it indeed achieved the highest transgene expression level despite the presence of serum. Comparing to PEG-*b*-PAEM block copolymers we reported earlier<sup>16</sup>, the PAEM homopolymers showed much higher transfection efficiency of DCs cultured in serum-free medium, presumably due to the fact that positively charged PAEM homopolymer/DNA polyplexes could be taken up by cells more efficiently. Another potential factor may be that although PEGylation is known to enhance colloidal stability of the polyplexes, too much stability might impede polyplex dissociation inside cells, hence resulting in lower gene transfection.

### DC maturation *in vitro* with and without serum

As a connection between the innate and adaptive immune responses, the maturation state of DCs is important to successful DNA vaccination. Several cationic polymers including polylysine derivatives<sup>33</sup>, PEI<sup>34</sup>, chitosan<sup>35</sup>, and poly(β-amino esters)<sup>36</sup> have been reported to enhance immune response, but the potential of inducing DC maturation by such cationic polymers has not been established. Here we examined the maturation state of murine DC 2.4 cells after treatment with PAEM/DNA polyplexes *in vitro*. As positive and negative controls, DCs treated with LPS up-regulated the expression of a maturation marker CD40, while naked DNA plasmid did not have any effect (Figure 9). Under serum-free conditions, exposure to the polyplexes at N:P ratios of 8 and 16 induced a strong up-regulation of CD40 at levels similar or higher than LPS, but the correlation between CD40 level and chain-length of PAEM was not pronounced (Figure 9). The presence of 10% serum in the cell culture media attenuated the amount of DC maturation at N:P ratio of 8 but not 16. At both N:P ratios, however, the correlation between polymer chain-length and DC maturation was apparent – polyplexes with longer PAEM chain-length caused higher up-regulation of CD40. These findings suggest that as carriers for DNA plasmid, the PAEM polymers may be potentially good adjuvants because of their ability of stimulating DC maturation, a prerequisite for generating adaptive immune responses. Furthermore, we have previously reported that PEG-*b*-PAEM block copolymers induced the maturation of murine bone marrow derived DCs in a chain-length-dependent manner<sup>16</sup>. It would be interesting to compare DC stimulatory capacity of the homopolymers with the PEG-block copolymers side-by-side. Regardless, it is speculated that such DC maturation stimulated by cationic polymers is at least partially due to the stress and cytotoxicity caused by the polymers<sup>21</sup>.

### Polyplex transfected DCs activated antigen-specific CD8<sup>+</sup> T cells *in vitro*

To assess the potential practical utility of the PAEM polymers for DNA vaccine delivery, we evaluated the ability of PAEM delivering a model antigen to activate naïve CD8<sup>+</sup> T cells. Twenty-four hours after transfecting DC 2.4 cells in the absence or presence of serum, naïve OVA-specific CD8<sup>+</sup> T cells harvested from mice were incubated with the DCs for 3 days. OVA-specific T cell activation was determined by quantifying the level of IFN-γ production. We found that under serum-free condition, polyplex-transfected DCs stimulated IFN-γ production by T cells at levels on par with the positive control – DCs stimulated with LPS and the CD8<sup>+</sup> T cell epitope from OVA, SIINFEKL peptide (Figure 10). The amount of IFN-γ production scaled with the level of gene transfection efficiency of DCs (Figure 8B), that is, at N:P ratio of 8, longer PAEM produced more IFN-γ, whereas at N:P ratio of 16, PAEM with the intermediate chain-length (DP = 75) resulted in the highest IFN-γ production (Figure 10). For DC transfection in the presence of serum, the IFN-γ level, once

again, correlated with the transfection efficiency under the same condition (Figure 8C), dropping to close to background level at N:P ratio of 8 and rebounding to approach the serum-free level at N:P ratio of 16 (Figure 10). Taken together, the correlation between polymer chain-length, transfection efficiency, and T cell activation was apparent. It is also a strong indication that the PAEM polymers may be potentially effective delivery vehicles of DNA vaccine for inducing antigen-specific T cell immunity. Further evaluation of the effectiveness of PAEM in DNA vaccination *in vitro* and *in vivo* is warranted.

PAEM is a structurally simple member of the poly(aminooalkyl methacrylate) family. It has a very flexible polymethacrylate backbone and high positive charge density at physiological pH, owing to the primary amine side-chains, which favors the formation of compact, nano-sized polyplexes. It would be interesting to see how further variations of the polymer structure might affect gene transfer and interaction with DCs, such as using longer alkyl chains between the charge center and the polymer backbone<sup>37,38</sup>. Also, a direct comparison between PAEM and a structurally similar yet more extensively studied gene carrier, PDMAEMA, which has tertiary amine side-chains<sup>39</sup>, may help understand the influence of the type of positive charge center on the formation and subcellular trafficking of polyplexes in DCs.

## CONCLUSIONS

Cationic PAEM polymers with precisely controlled chain-length were synthesized and characterized for delivering plasmid DNA to antigen-presenting dendritic cells. Through a comprehensive study we revealed correlations between polymer chain-length and colloidal properties of the polyplexes, transfection efficiency, uptake in dendritic cells and subcellular trafficking, and the capacity of inducing DC maturation and CD8<sup>+</sup> T cell activation by a model DNA vaccine. Thus, the structurally simple and defined PAEM polymer is not only a useful model material for understanding structure-function relationship in nonviral gene delivery, but may also be a practically effective, immunostimulatory DNA vaccine carrier.

## Supplementary Material

Refer to Web version on PubMed Central for supplementary material.

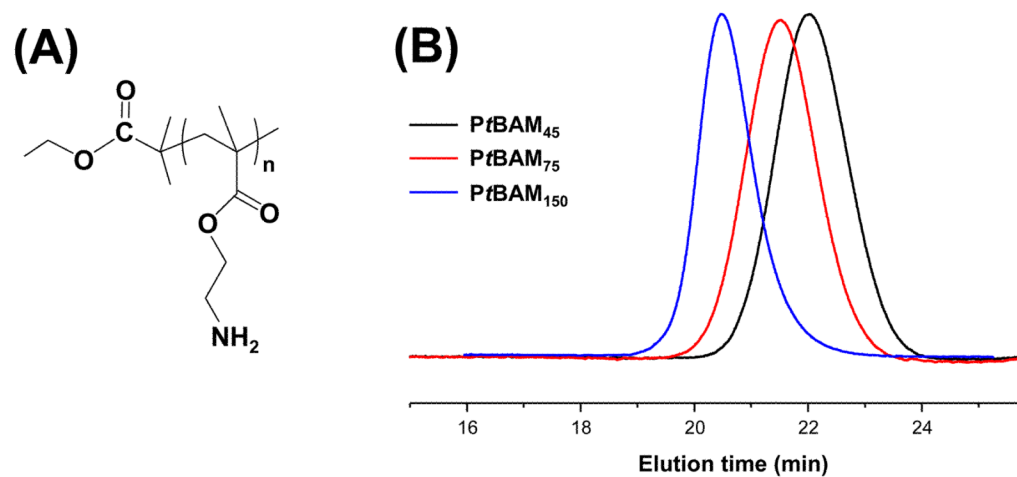
## Acknowledgments

The authors thank Dr. John Ohlfest for providing the DC 2.4 cells, Dr. Matt Mescher for providing the OT-1/PL mice, Dr. Robert Tranquillo for the use of fluorescence plate reader, Dr. Marc Hillmyer for the use of the GPC system, and the Biomedical Imaging Processing Laboratory (BIP) at the University of Minnesota for assistance with confocal microscopy and image quantification. C. Wang acknowledges the support by the NSF (grant BES0547613), the NIH (grant R01CA129189), and the DOD (through a subcontract grant WU-07-151/W81XWH-06-1-0677 by Washington University at St. Louis). R. Tang acknowledges the support by the Chinese Program for New Century, Excellent Talents in Universities (No. NCET-10-0435), the National Natural Science Foundation of China (No. 21004030, 50873080), the Natural Science Foundation of Jiangsu Province of China (No. BK2010145), and the Fundamental Research Funds for the Central Universities of China (JUSRP21013).

## References

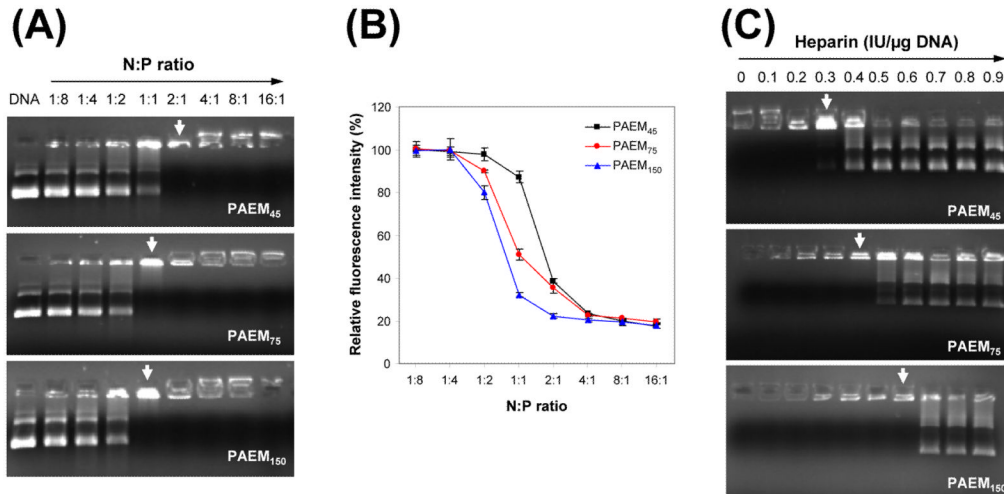
1. Ladd DJ, Weiner DB. *Int Rev Immunol*. 2006; 25:99–123. [PubMed: 16818367]
2. Mellman I, Steinman RM. *Cell*. 2001; 106:255–258. [PubMed: 11509172]
3. Rock KL, Shen L. *Immunol Rev*. 2005; 207:166–183. [PubMed: 16181335]
4. Pack DW, Hoffman AS, Pun S, Stayton PS. *Nat Rev Drug Discov*. 2005; 4:581–593. [PubMed: 16052241]
5. Mintzer MA, Simanek EE. *Chem Rev*. 2009; 109:259–302. [PubMed: 19053809]
6. Wong SY, Pelet JM, Putnam D. *Prog Polym Sci*. 2007; 32:799–837.

7. Nguyen DN, Green JJ, Chan JM, Longer R, Anderson DG. *Adv Mater.* 2009; 21:847–867.
8. Godbey WT, Wu KK, Mikos AG. *J Biomed Mater Res.* 1999; 45:268–275. [PubMed: 10397985]
9. Layman JM, Ramirez SM, Green MD, Long TE. *Biomacromolecules.* 2009; 10:1244–1252. [PubMed: 19331402]
10. Srinivasachari S, Liu YM, Prevette LE, Reineke TM. *Biomaterials.* 2007; 28:2885–2898. [PubMed: 17367850]
11. Ren Y, Jiang XA, Pan D, Mao HQ. *Biomacromolecules.* 2010; 11:3432–3439. [PubMed: 21067136]
12. Breunig M, Lungwitz U, Liebl R, Fontanari C, Klar J, Kurtz A, Blunk T, Goepferich A. *J Gene Med.* 2005; 7:1287–1298. [PubMed: 15906395]
13. Morimoto K, Nishikawa M, Kawakami S, Nakano T, Hattori Y, Fumoto S, Yamashita F, Hashida M. *Mol Ther.* 2003; 7:254–261. [PubMed: 12597914]
14. Matyjaszewski K, Xia JH. *Chem Rev.* 2001; 101:2921–2990. [PubMed: 11749397]
15. Heath WH, Senyurt AF, Layman J, Long TE. *Macromol Chem Phys.* 2007; 208:1243–1249.
16. Tang RP, Palumbo RN, Nagarajan L, Krogstad E, Wang C. *J Control Release.* 2010; 142:229–237. [PubMed: 19874858]
17. Kuroda K, DeGrado WF. *J Am Chem Soc.* 2005; 127:4128–4129. [PubMed: 15783168]
18. Mosmann T. *J Immunol Methods.* 1983; 65:55–63. [PubMed: 6606682]
19. Godbey WT, Wu KK, Mikos AG. *Proc Natl Acad Sci USA.* 1999; 96:5177–5181. [PubMed: 10220439]
20. Akita H, Ito R, Khalil IA, Futaki S, Harashima H. *Mol Ther.* 2004; 9:443–451. [PubMed: 15006612]
21. Palumbo RN, Zhong X, Wang C. *J Control Release.* 201110.1016/j.jconrel.2011.08.037
22. Dufresne MH, Leroux JC. *Pharm Res.* 2004; 21:160–169. [PubMed: 14984271]
23. Dufresne MH, Elsabahy M, Leroux JC. *Pharm Res.* 2008; 25:2083–2093. [PubMed: 18452054]
24. Dubruel P, Christiaens B, Rosseneu M, Vandekerckhove J, Grooten J, Goossens V, Schacht E. *Biomacromolecules.* 2004; 5:379–388. [PubMed: 15002997]
25. Zhu CH, Jung S, Si GY, Cheng R, Meng FH, Zhu XL, Park TG, Zhong ZY. *J Polym Sci Polym Chem Ed.* 2010; 48:2869–2877.
26. He LH, Read ES, Armes SP, Adams DJ. *Macromolecules.* 2007; 40:4429–4438.
27. Manolova V, Flace A, Bauer M, Schwarz K, Saudan P, Bachmann MF. *Eur J Immunol.* 2008; 38:1404–1413. [PubMed: 18389478]
28. Funhoff AM, van Nostrum CF, Koning GA, Schuurmans-Nieuwenbroek NME, Crommelin DJA, Hennink WE. *Biomacromolecules.* 2004; 5:32–39. [PubMed: 14715005]
29. Jones NA, Hill IRC, Stolnik S, Bignotti F, Davis SS, Garnett MC. *Biochim Biophys Acta-Gene Struct Express.* 2000; 1517:1–18.
30. Dash PR, Read ML, Barrett LB, Wolfert M, Seymour LW. *Gene Ther.* 1999; 6:643–650. [PubMed: 10476224]
31. Guo WJ, Lee RJ. *J Control Release.* 2001; 77:131–138. [PubMed: 11689266]
32. Kuo JHS. *Biotechnol Appl Biochem.* 2003; 37:267–271. [PubMed: 12597775]
33. Locher CP, Putnam D, Langer R, Witt SA, Ashlock BM, Levy JA. *Immunol Lett.* 2003; 90:67–70. [PubMed: 14687705]
34. Lisziewicz J, Trocio J, Whitman L, Varga G, Xu JQ, Bakare N, Erbacher P, Fox C, Woodward R, Markham P, Arya S, Behr JP, Lori F. *J Invest Dermatol.* 2005; 124:160–169. [PubMed: 15654970]
35. Roy K, Mao HQ, Huang SK, Leong KW. *Nat Med.* 1999; 5:387–391. [PubMed: 10202926]
36. Greenland JR, Liu HN, Berry D, Anderson DG, Kim WK, Irvine DJ, Langer R, Letvin NL. *Mol Ther.* 2005; 12:164–170. [PubMed: 15963932]
37. Ke JH, Wei MF, Shieh MJ, Young TH. *J Biomater Sci-Polym Ed.* 2011; 22:1215–1236.
38. Wong SY, Sood N, Putnam D. *Mol Ther.* 2009; 17:480–490. [PubMed: 19142180]
39. Tao L, Liu JQ, Tan BH, Davis TP. *Macromolecules.* 2009; 42:4960–4962.

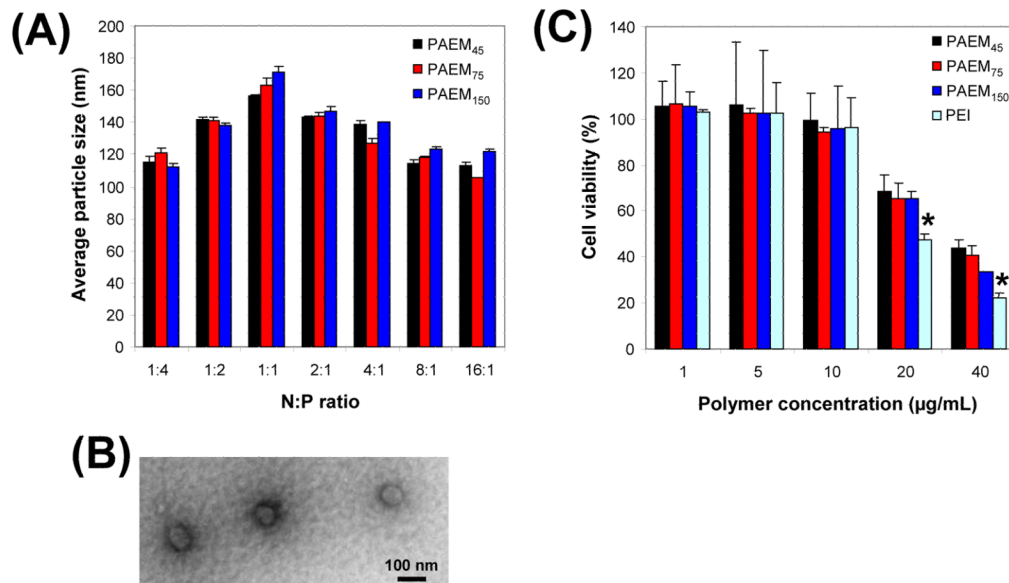


**Figure 1.**

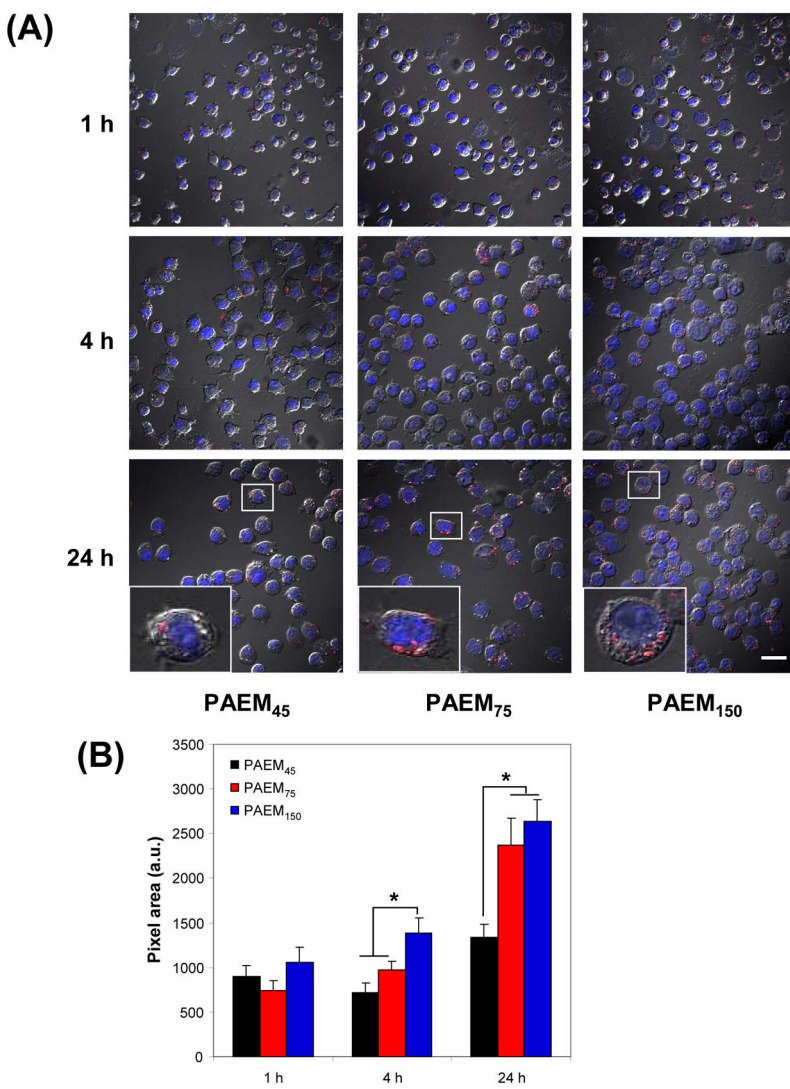
(A) Chemical structure of the PAEM polymer. (B) GPC traces of PtBAM, the precursor of PAEM with Boc-protected side-chains, using CHCl<sub>3</sub> as mobile phase and a flow rate of 1 mL/min. Average molecular weight was determined based on polystyrene standards.

**Figure 2.**

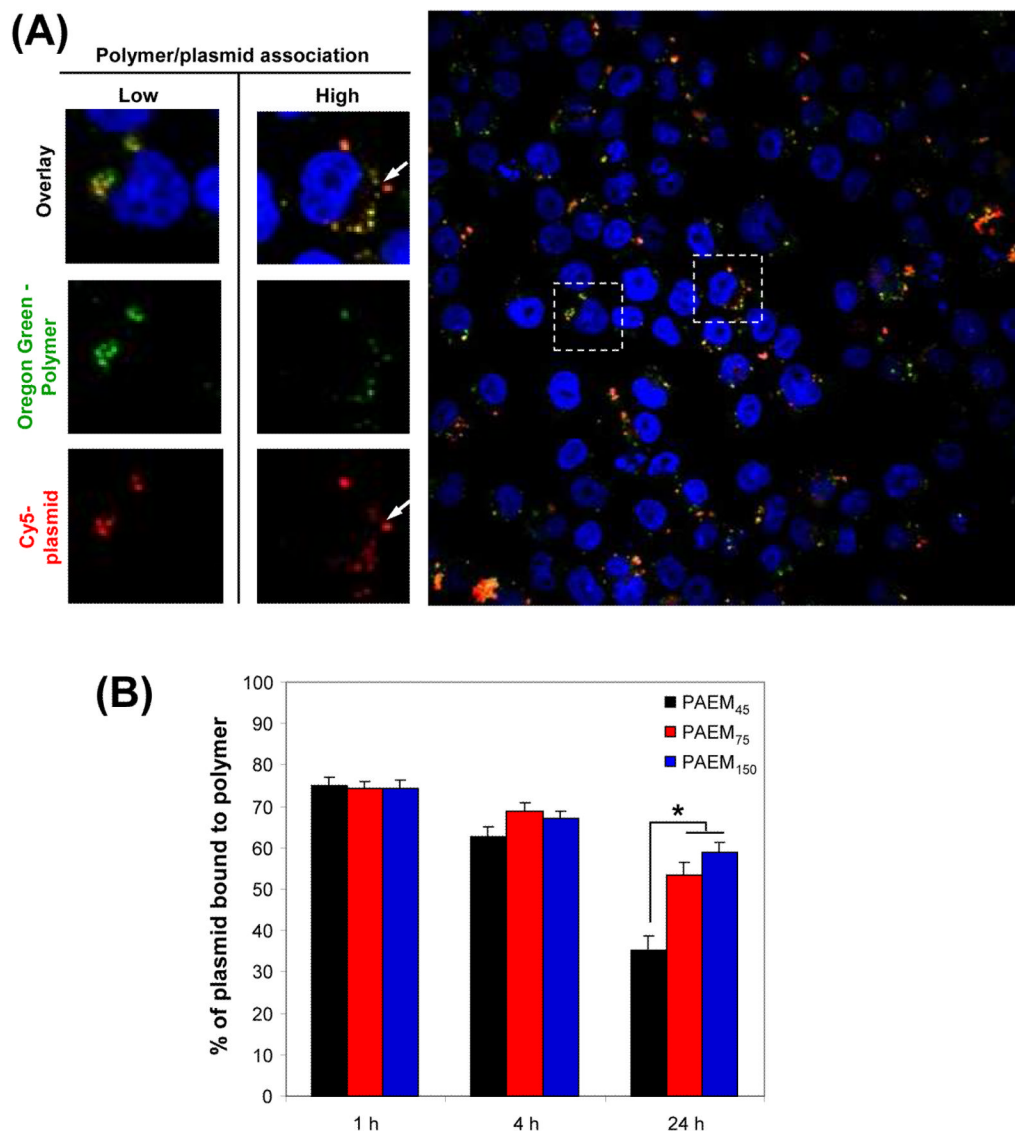
The capacity of DNA binding and condensation by the PAEM polymers with different chain-length. (A) Gel retardation assay of polyplexes prepared at various N:P ratios. Arrows point to the threshold N:P ratio where retardation of DNA migration through the gel occurred. (B) Ethidium bromide (EB) exclusion due to polyplex formation. Fluorescence intensity of EB mixed with plasmid without addition of polymer was taken as 100%. (C) Destabilization of polyplexes with increasing concentration of heparin. Arrows point to the threshold concentration of heparin beyond which unpackaging of DNA occurred.

**Figure 3.**

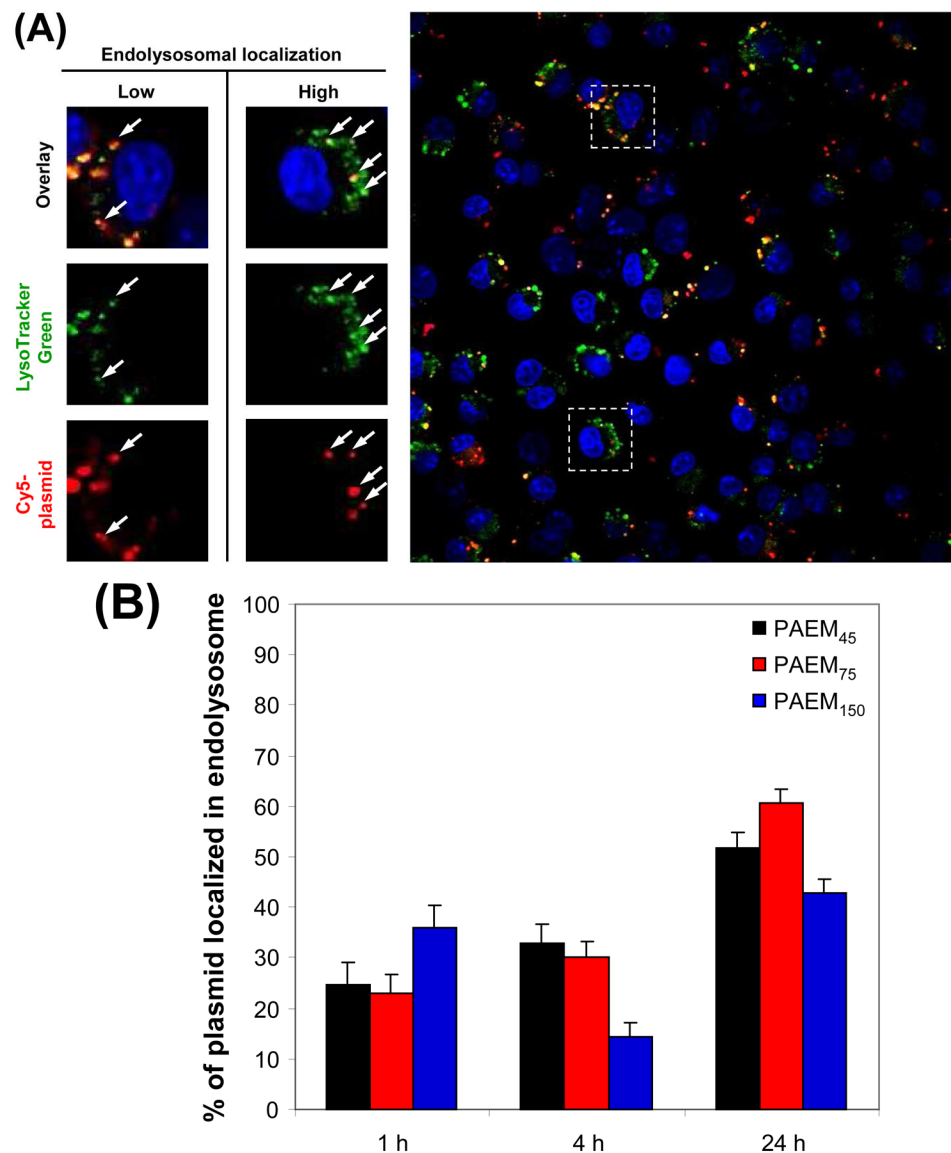
Average particle size of the polyplexes and cytotoxicity. (A) Average particle size of polyplexes in aqueous buffer (20 mM HEPES, pH 7.4) as a function of N:P ratio determined by DLS. (B) A typical TEM image of polyplexes (N:P ratio of 8) showing discrete, condensed nanoparticles of ~100 nm in size. Scale bar: 100 nm. (C) Cytotoxicity of PAEM polymers to DC 2.4 cells measured by the MTT assay. Viability of cells cultured without polymer was taken as 100%. \*  $p<0.05$ , compared with PAEM polymers at equivalent concentrations.

**Figure 4.**

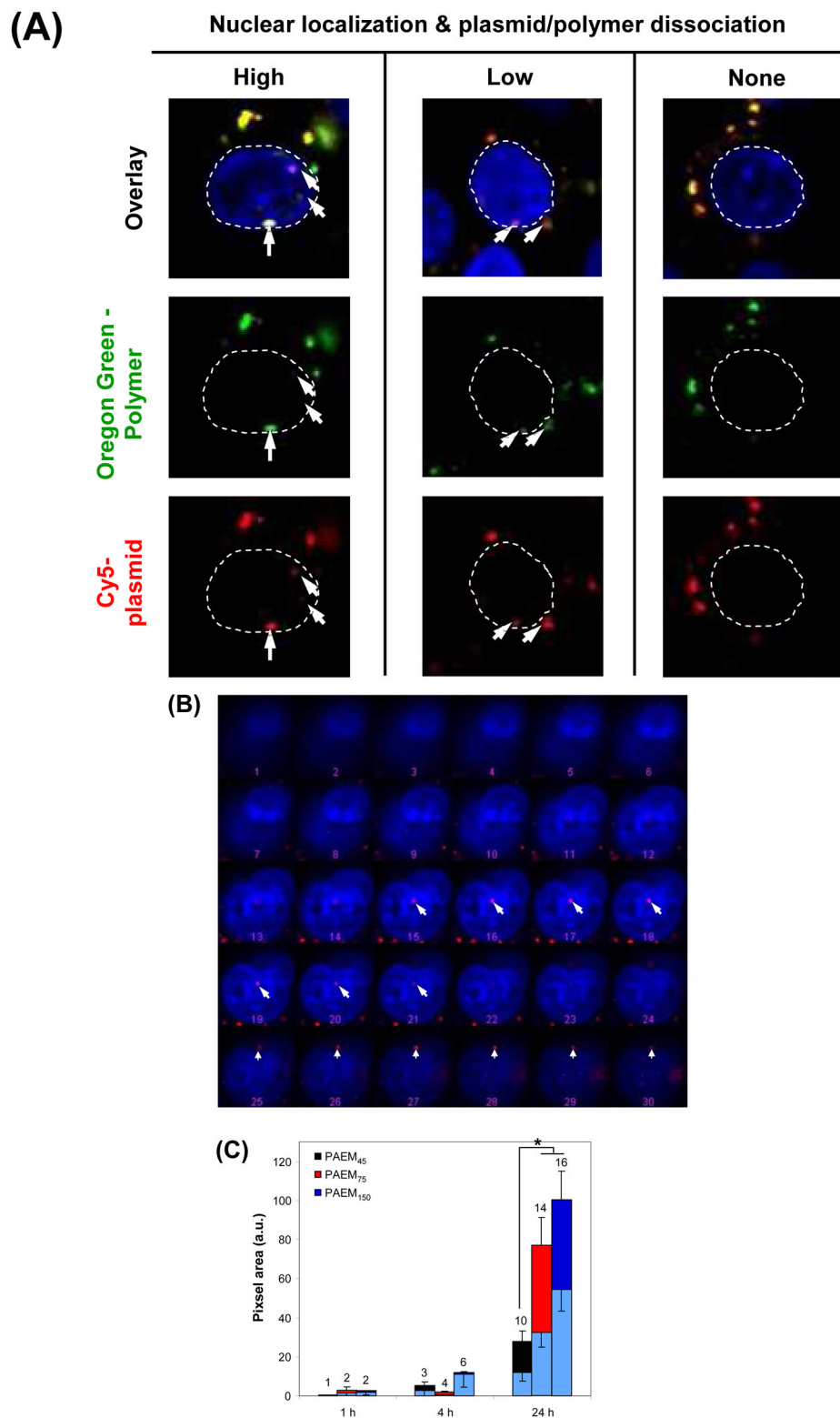
Cellular uptake of plasmid. (A) Representative confocal fluorescence microscopy images of DC 2.4 cells transfected by polyplexes (N:P ratio of 8) at various time points. Red: Cy5-labeled plasmid. Blue: Hoechst 33342 staining cell nuclei. Shown are fluorescence overlaid with white-light images. Scale bar: 25  $\mu$ m. (B) Quantification of cellular uptake. Mean  $\pm$  SE, 30 cells for each sample were counted, \* $p$ <0.05.

**Figure 5.**

Intracellular dissociation of polyplexes. (A) Representative confocal fluorescence microscopy images of DC 2.4 cells transfected by polyplexes (N:P ratio of 8) at 24 h. Red: Cy5-labeled plasmid. Green: Oregon Green-labeled polymer. Blue: Hoechst 33342 staining cell nuclei. Arrows point to polyplexes that remained intact or dissociated (labeled “low” or “high”, respectively). (B) Quantification of intracellular polyplex dissociation. Mean  $\pm$  SE, 30 cells for each sample were counted, \* $p$ <0.05.

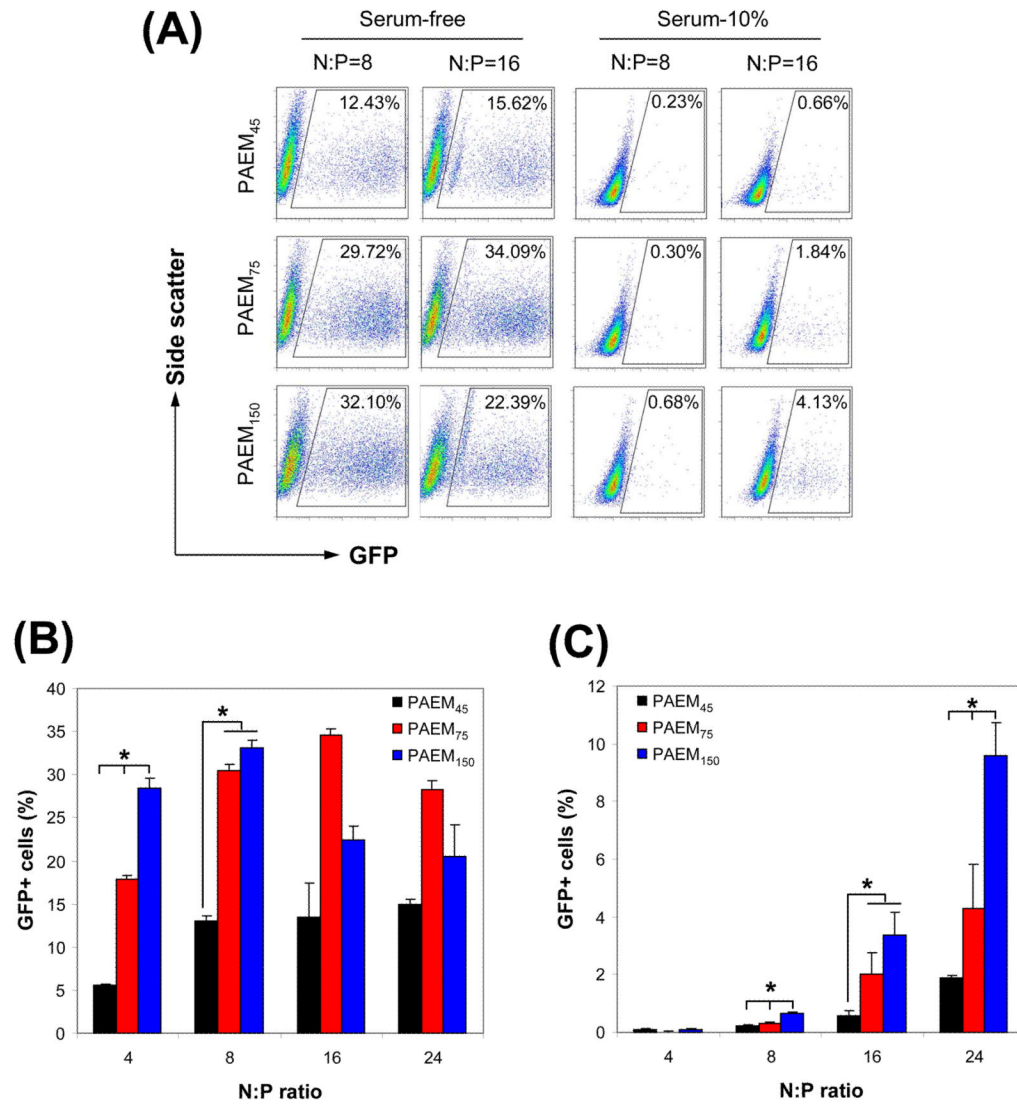
**Figure 6.**

Endolysosomal localization of plasmid. (A) Representative confocal fluorescence microscopy images of DC 2.4 cells transfected by polyplexes (N:P ratio of 8) at 24 h. Red: Cy5-labeled plasmid. Green: LysoTracker Green. Blue: Hoechst 33342 staining cell nuclei. Arrows point to regions where plasmid was or was not localized in the endolysosome (labeled “high” or “low, respectively). low degree of localization plasmid that remained intact (low) or dissociated (high). (B) Quantification of plasmid localized in the endolysosome. Mean  $\pm$  SE, 30 cells for each sample were counted, \* $p$ <0.05.

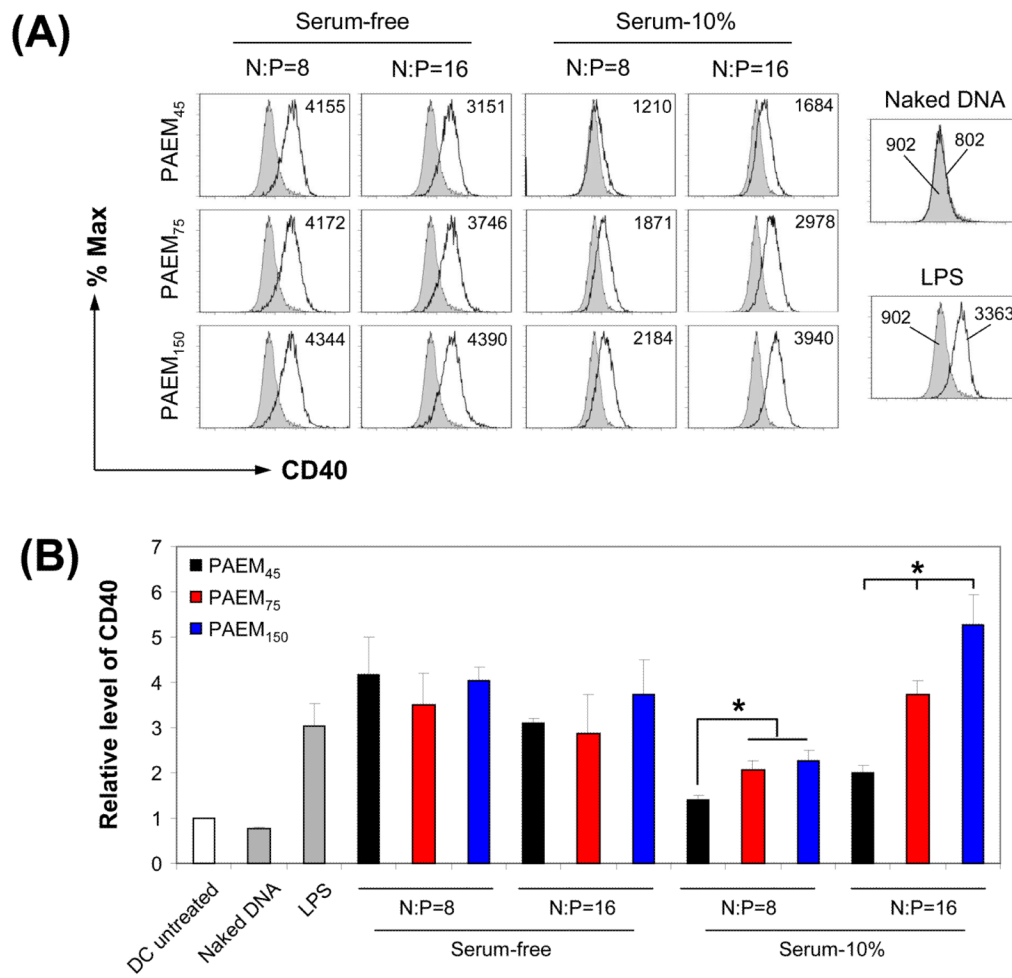
**Figure 7.**

Nuclear localization of plasmid and dissociation of polyplexes. (A) Representative confocal fluorescence microscopy images of DC 2.4 cells transfected by polyplexes (N:P ratio of 8) at

24 h. Red: Cy5-labeled plasmid. Green: Oregon Green-labeled polymer. Blue: Hoechst 33342 staining cell nuclei outlined in dotted white lines. Arrows point to regions where plasmid signal was found in the nucleus.

**Figure 8.**

Transfection efficiency of DC 2.4 cells by polyplexes determined by flow cytometry. (A) Representative dot plots of transfected cells. The GFP<sup>+</sup> gate was set based on cells transfected with a luciferase plasmid (Figure S3). (B,C) Quantification of the percentage of GFP<sup>+</sup> cells transfected in the absence (B) or presence (C) of 10% serum. \* $p<0.05$ .

**Figure 9.**

Maturation of DC 2.4 cells by polyplexes marked by upregulation of CD40. (A) A representative set of flow cytometry data of cells transfected by polyplexes or LPS or naked DNA only, in the presence or absence of serum. The shaded area is untreated DCs. Numbers represent the values of mean fluorescence intensity. (B) Quantification of DC maturation. CD40 level was normalized against untreated DCs. \* $p<0.05$ .

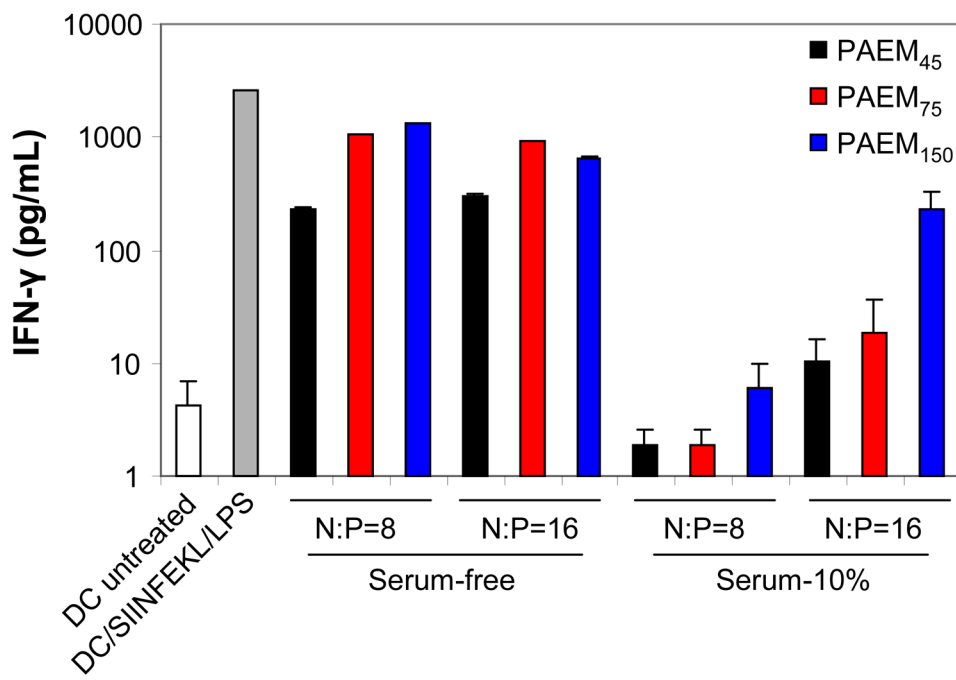


**Figure 10.**

CD8<sup>+</sup> T cell activation. DCs were transfected with polyplexes containing a model antigen (OVA) encoding plasmid in the absence or presence of serum. Untreated DCs and DCs stimulated with SIINFEKL peptide plus LPS were used as controls. IFN- $\gamma$  production by CD8<sup>+</sup> OVA-specific T cells was quantified by ELISA.